Condensation of Water Vapor in Rarefaction Waves III. Experimental Results

I. I. Glass,* S. P. Kalra,† and J. P. Sislian‡
University of Toronto, Toronto, Canada

An experimental investigation is presented of nonequilibrium condensation in a nonstationary rarefaction wave of water vapor-nitrogen mixtures. Density and pressure variations as well as the onset of condensation due to such expansions were monitored at two fixed locations in the driver section of a 2.5 cm × 2.5 cm shock tube by using a laser Fabry-Perot interferometer, a differential interferometer and piezotron transducers. The effects of the cooling rate on the supersaturation (or supercooling) at the onset of condensation were determined through an empirical relation. An analysis using this relation predicted the path of the condensation front in such rarefaction waves for a set of initial conditions given by: 1) relative humidity ϕ_4, 2) vapor mass fraction ω_4, and 3) temperature T_4. The experimental data were found to be in general qualitative agreement with the simple analytical predictions.

Introduction

CONDENSATION phenomena during expansions in shock tubes and nozzles have been investigated by a number of authors.[1-4] The exothermic character of these processes places them in close relation to flows involving chemical reactions. The application of a shock tube to condensation studies was initiated by Wegener and Lundquist[5] and used later by Glass and Patterson,[6] Homer,[7] Kung and Bauer,[8] Kawada and Mori,[9] and Barschdorff.[10]

If the vapor of any substance is suddenly cooled by an expansion process there is some time t, at which the vapor becomes saturated and then follows a supersaturated state in which nonequilibrium condensation begins. It is well known that condensation is greatly facilitated by the presence of foreign particles that become condensation centers about which liquid drops form (heterogeneous-nucleation model).[11] However, in an ideally pure supersaturated vapor, condensation centers appear as a result of the agglomeration of molecules into molecular complexes (homogeneous-nucleation model).[12] After reaching the so-called critical size, the complexes become stable and do not break up, and exhibit a tendency for further growth and transformation into droplets.[13] The rate of formation of condensation centers has an extremely strong dependence on the degree of supersaturation. The number of condensation centers depends on the maximum attainable supersaturation and is determined by the interplay of two opposing effects, namely, the cooling of the vapor, corresponding to the work of expansion, and its heating resulting from the release of the latent heat of condensation.

The present paper first describes some experimental results obtained from a study of the nonequilibrium condensation of water vapor and nitrogen mixtures in a nonstationary rarefaction wave produced in a shock tube. The condensation results provided the basis for an empirical relation between the supercooling and the rate of cooling at the onset of condensation. Although this relation was useful in the analysis of the location of the path of the condensation front in the rarefaction fan as a function of the initial conditions in the driver section, it is not in agreement with the predictions of the relations between supercooling and cooling rate given by the models of heterogeneous and homogeneous nucleation described in Parts I and II of this series.[11,12] Nevertheless, this paper provides the experimental basis and data used in these two parts.

Received Oct. 5, 1976; revision received Feb. 9, 1977.
Index categories: Multiphase Flows; Nozzle and Channel Flow; Shock Waves and Detonations.

*Professor, Institute for Aerospace Studies. Fellow AIAA.
†Research Engineer, Atomic Energy of Canada Limited, Chalk River Nuclear Laboratories, Advance Engineering Branch, Chalk River, Ontario.
‡Research Associate. Institute for Aerospace Studies. Member AIAA.

Experimental Facility

A 2.5 × 2.5 cm shock tube facility was designed and built at the Institute for Aerospace Studies in order to investigate nonstationary, nonequilibrium condensation phenomena of water vapor-nitrogen mixtures. Two techniques were used to inject the water vapor into the system: 1) by exposing water surfaces to vacuum, 2) by bubbling the ultra-pure nitrogen carrier gas through ultra-pure water. (Ultra-pure nitrogen is available commercially and contains gas impurities up to a few parts per million; similarly, ultra-pure water is practically free of contaminants.) The first method was found to be more convenient and reliable. It also permitted easy measurements of initial vapor pressure and temperature required for relative humidity calculations. It is estimated that the errors in the initial vapor pressure and temperature measurements are about 2%.

Measurements were performed at two locations in the driver section of the shock tube at $x_1 = -17.1$ cm and at $x_2 = -35.1$ cm. The parameters monitored were density, density gradient, pressure, and the onset of condensation. Two laser interferometers and two piezotron transducers were used for this purpose. A brief description of these techniques follows.

An external Fabry-Perot (F-P) cavity was formed using two optical semitransparent flats (flatness $\approx \lambda/50$). The beam was folded within the cavity in order to increase the measurement sensitivity threefold by making three passes through the test section. The transmitted intensity I_T of the laser light through the external F-P cavity is a function of the losses within the cavity and can be expressed by

$$\frac{I_T}{I_0} = \frac{1}{1+F\sin^2(\delta/2)} \tag{1}$$

where I_0 is the input intensity of the laser radiation and F is defined by

$$F = 4R_{ef}/(1-R_{ef})^2 \tag{2}$$

and is determined by losses within the cavity which are defined by the effective reflectivity of the cavity R_{ef}. The

value of F is constant for a given Fabry-Perot cavity. Normalizing the above[14]

$$\bar{I}_s = \frac{\cos^2(\delta/2)}{1+F\sin^2(\delta/2)} \tag{3}$$

The value of $\bar{I}_s$ varies from 1 to 0 as δ varies from 0 to π (corresponding to half a fringe shift). The intensity $\bar{I}_s$ is modulated with time in accordance with the phase δ, which changes linearly with density such that

$$\delta(t) = 6\pi\, KL\, \rho(t)/(\lambda/2) \tag{4}$$

where K is the Gladstone-Dale constant, L is the width of the test section, λ is the He-Ne laser wavelength (6328 Å) and $\rho(t)$ is the density at each instant of time. Therefore, measurements of modulation of intensity within the F-P cavity can be used to determine the vapor-density profiles through a rarefaction wave. These intensity modulations were measured by a photomultiplier tube (EMI 9558B). The alignment procedure, calibration and fractional fringe measurements are described in detail in Ref. 14.

A differential interferometer was designed by splitting the laser beam into two closely-spaced parallel beams (separation ≈ 1 mm) and then recombining them with another similar splitter. This system is similar to the two beams of a Mach-Zehnder interferometer. It registers the phase change between the beams, which is essentially proportional to the density change occurring within 1 mm distance (i.e., a sharp gradient in density). In addition to the measurements of density and density gradients, these optical devices give very accurate records of the onset of condensation as a result of phase change into liquid droplets which act as scattering sources for the laser light; therefore the output intensities of these interferometric devices would show a sudden change (spatial resolution ≈ 1 mm; time resolution ≈ 50 nsec, i.e., limits of the recording device). Also two low-pressure piezotron transducers (Kistler Model 206) were used at the same two locations to monitor the pressure profiles.

The opening time of the shock-tube diaphragm was monitored optically by having the laser light fall on a photodiode at the instant of rupture. The photodiode was wired to a device which triggered the oscilloscopes, thus giving an accurate zero-time reference for the traces. A schematic of the condensation-shock-tube facility and its associated optical sensors is shown in Fig. 1. A sketch of the experimental arrangement and a time-distance (x,t)-plot of the wave motion and experimental traces are shown in Fig. 2. The two traces of oscilloscope no. 1 show variations in pressure (upper trace) and density gradient (lower trace) at $x_1 = -17.1$ cm from the diaphragm station, in the driver-section of the shock tube. Corresponding traces of oscillograph no. 2 represent pressure and density changes, respectively, at $x_2 = -35.1$ cm. A sudden change in the traces shows the arrival time of the condensation front at these locations.

Condensation in a Rarefaction Wave

A schematic diagram illustrating the nonequilibrium condensation flow in a weak rarefaction wave from the instant of diaphragm rupture in a shock tube in the (x,t)-plane is shown in Fig. 3. The resulting pressure profiles at two locations (x_1 and x_2) through the rarefaction fan as a function of time are also indicated for clarity. An initially planar centered rarefaction wave is assumed in this illustration.

The straight lines (characteristics) are the trajectories of constant gas properties. The adiabatic cooling of the mixture (water-vapor-N_2 gas) begins at the wave head H, where the temperature gradient has a maximum. The characteristic s corresponds to equilibrium condensation with pressure P_s and temperature T_s, and is called the saturation characteristic. Owing to the rate processes involved, no condensation takes place at this saturation characteristic,[13] and the mixture expands further along the particle path with increasing supersaturation until it reaches the front O, where due to the collapse of the metastable state (critical state) condensation occurs spontaneously.[13] The latent heat released causes the pressure to increase very rapidly to a peak value thereby forming a condensation front S_c, which may or may not be followed by a shock wave.[12] The condensation front in the rarefaction fan originates at the tail T of the wave where the temperature is at the lowest value and propagates in a manner such that its slope tends toward the saturation characteristic with increasing distance from the diaphragm (owing to the monotonic decrease of the cooling rate).

Actual schlieren (x,t)-plane records[6] are shown in Fig. 4, for stronger rarefaction waves, where the tail of the wave lies

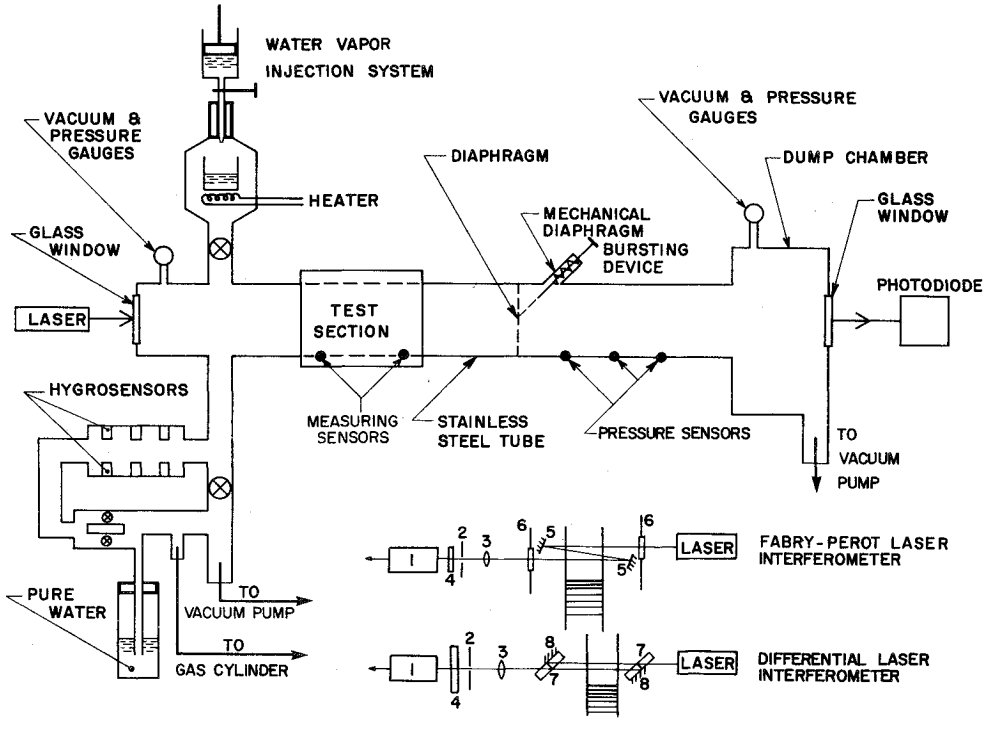

Fig. 1 Schematic diagram of condensation-shock-tube facility and associated optical sensors 1) photomultiplier, 2) pinhole, 3) lens, 4) optical filter, 5) beam folding mirrors, 6) F. P. flats (λ/50 flatness), 7) beam splitter, 8) mirrors; shock tube cross-section 2.5 cm × 2.5 cm.

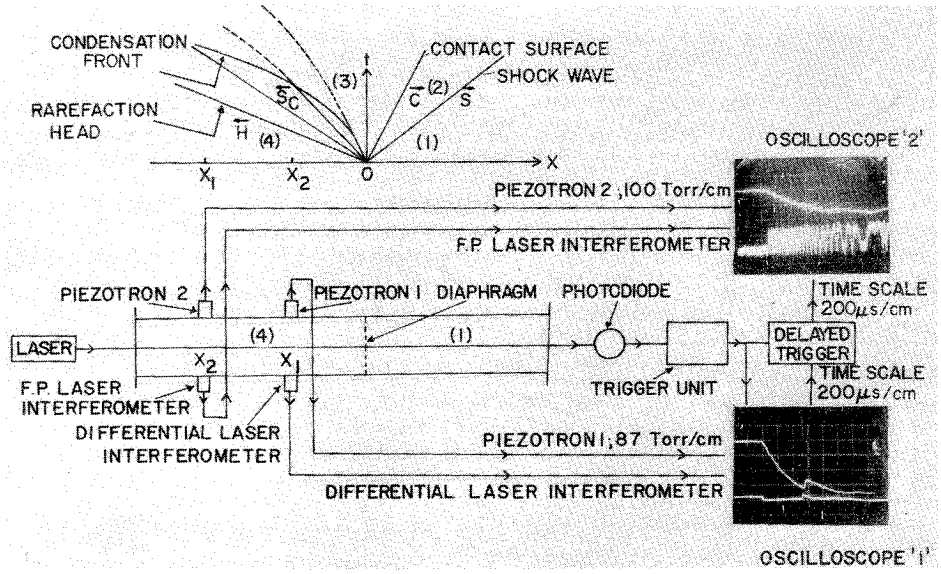

Fig. 2 Schematic diagram of experimental arrangements, type of oscilloscope traces, and an x-t plane diagram of the wave system.

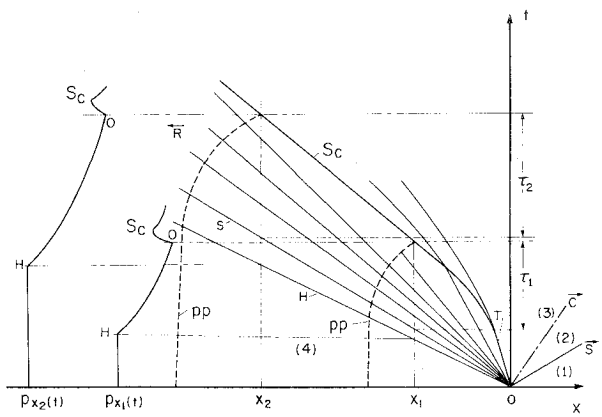

Fig. 3 Schematic diagram of the x-t plane showing the path of a condensation front in an initially centered rarefaction wave and the corresponding pressure profiles at two locations in a shock tube. R = rarefaction wave, H = wave head, S_c = condensation front, s = saturation characteristic, T = wave tail, 0 = onset of condensation, pp = particle paths, τ_1 = condensation delay time at x_1, τ_2 = condensation delay time at x_2, C = contact surface, S = shock wave, initial states 4, 1; quasisteady states 3,2.

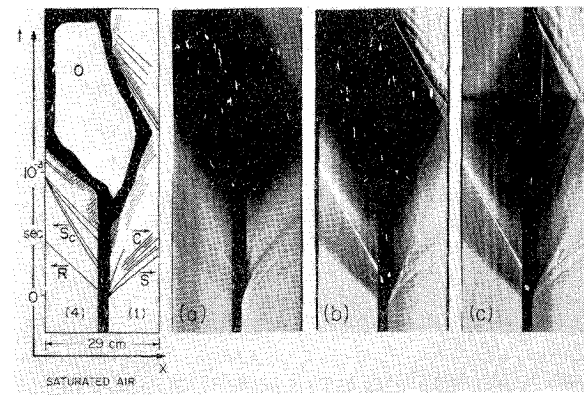

Fig. 4 Schlieren photographs of the distance-time (x-t) plane of the flow at the origin in a 7.6 cm × 7.6 cm shock tube with saturated air as the driver gas and the channel containing air, R = rarefaction wave, S_c = condensation shock wave, 0 = opaque condensation region, C = contact front region, S = primary shock wave. Only the diaphragm pressure ratios P_{41} differ in records a), b), and c), 10, 25, and 50, respectively. The initial conditions in the driver are the same. P_4 = 746 torr, T_4, T_1 = 297K φ_4 = 100% calculated, ω_4 = 1.8%. As expected, the condensation shock wave paths are the same and all of them start to the right of the t-axis. The actual starting point is masked by the rupturing diaphragm.

to the right of the t-axis. The start of the condensation front at the wave tail is therefore obscured. As expected, the condensation front velocity is independent of diaphragm pressure ratio for a given set of driver conditions.[12] Actual pressure records as well as density and density gradient traces are shown in Fig. 5.

In practice, owing to tube geometry, the nonideal and finite rupturing process of the curved diaphragm and effects due to the viscous boundary layer (has a negligible effect with a thickness of about 0.2 mm at the measuring station), the wave is initially neither centered nor planar.[15] In line with the work of Kawada and Mori,[9] the waves in the present experiments also were found to be noncentered. Nevertheless, from a comparison of the measured pressure profiles at the two locations with those predicted for planar centered rarefaction waves, it has been found that the agreement is, on the whole, reasonably good. Therefore the local particle velocities for ideal waves may be computed from the measured pressure or density profiles.[15]

The transucers at the two locations made it possible to measure the speed of sound in a mixture from the head of the rarefaction wave.[16] Using the measured speed of sound, a correction can be applied to the present noncentered waves in order to make them equivalent to centered waves.[17] Barrand and Rieutord[18] found that rarefaction waves in a moist gas in a shock-tube channel approached a planar-wave profile when they used a sufficiently large length-to-diameter ratio $(L/D) \sim 23$. However, the cooling rates for such distant locations become small and a comparison with predicted nonequilibrium condensation processes becomes difficult. In the present study, the observation stations were located at ~7 and ~14 hydraulic diameters. Although the waves were probably not centered, the nonequilibrium phenomena could be observed with ease.

Experimental Results

The initial conditions for a selected number of runs are given in Table 1. The values of relative humidity ϕ_4 varied from 60 to 97%. A wider range of initial temperature T_4 and water-vapor mass fraction in the driver ω_4 was not possible due to the lack of an external heater. The sound velocity a_4 of the water vapor-N_2 mixture was computed using the following relations[12]

$$a_4^2 = \gamma_4 (R/\mu_4) T_4 \qquad (5)$$

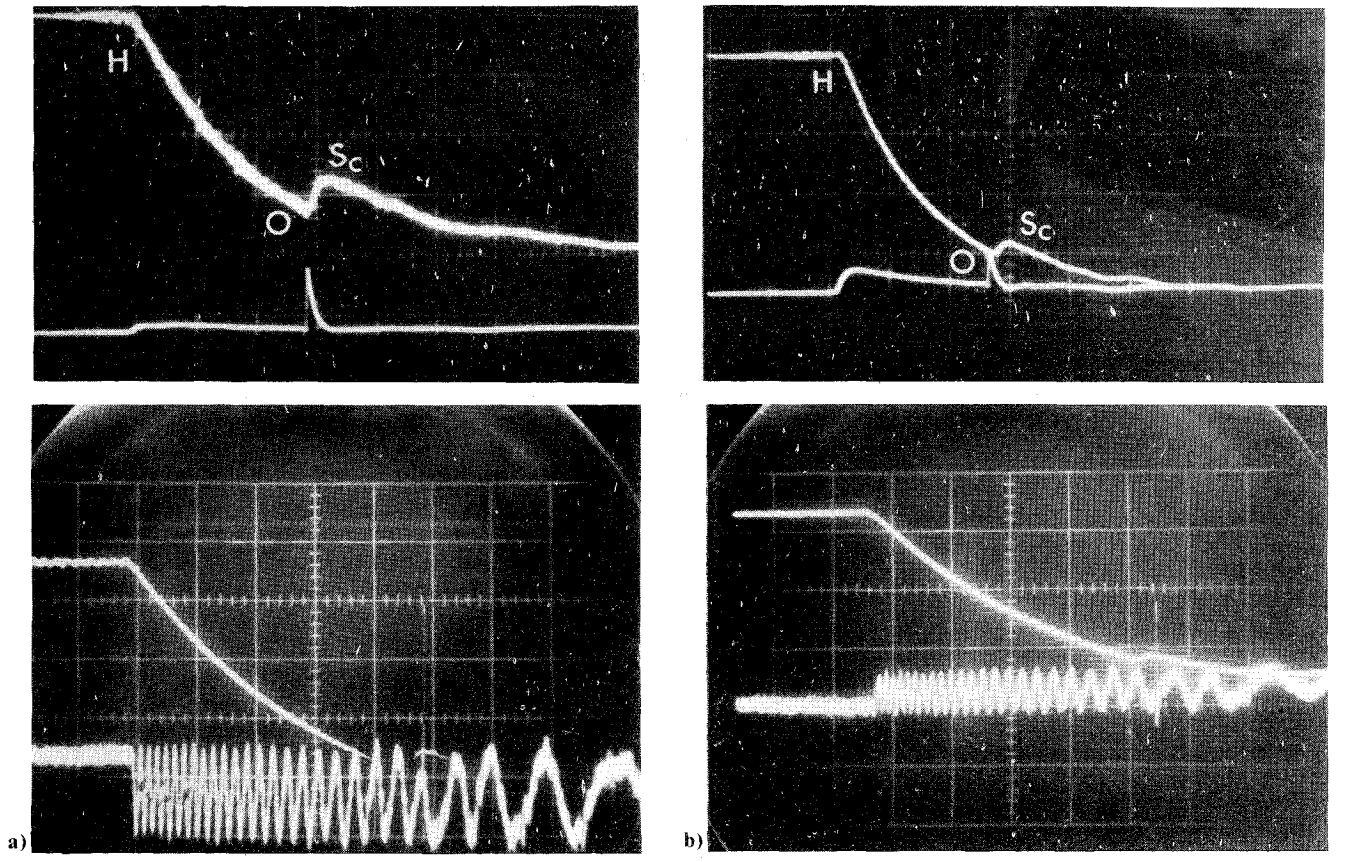

Fig. 5 Some experimental results showing pressure, density, and density gradient traces recorded at 200 μsec/cm with 500 μsec delay between the two locations x_1 and x_2, a) $P_4 = 680$ Torr, $\varphi_4 = 92\%$, $T_4 = 293$K, b) $P_4 = 680$ Torr, $\varphi_4 = 61.7\%$, $T_4 = 293$K.

where

$$\gamma_4 = \frac{(1-\omega_4)C_{pN_2} + \omega_4 C_{pV}}{(1-\omega_4)C_{vN_2} + \omega_4 C_{vV}} \tag{6}$$

and

$$\frac{1}{\mu_4} = \frac{1-\omega_4}{\mu_{N_2}} + \frac{\omega_4}{\mu_V} \tag{7}$$

where C_p and C_v are the specific heats for water-vapor and N_2 at constant pressure and volume, respectively.

In Table 2 both calculated and measured sound velocities from the rarefaction-wave head[16] are given. The agreement is excellent. The sound velocities at the saturation temperature, which were determined from the intersection points of the saturation curve with the experimental isentrope, are also listed for completeness.

The calculated (based on centered-wave theory[15]) and experimental pressure profiles are plotted in Fig. 6. It can be seen that some deviation from the predicted profiles occurs. This has been discussed in detail in Ref. 12, where it is shown that for a particular case the digitized experimental profile at $x_1 = -17.1$ cm is best fitted by one that corresponds to $x = -23.4$ cm from the diaphragm.

The onset conditions for the selected number of runs are shown in Table 1. It can be seen from this table that the larger values of supersaturation S at the onset are found at the location closer to the diaphragm where the rates of cooling are high. In Fig. 7, S, at both locations, is plotted vs the condensation delay time τ (calculated from the equilibrium state in laboratory coordinates). Mean values of τ were estimated as indicated. The spontaneous condensation at the onset takes place within about 30 μsec, compared to the relatively long condensation delay times, 490 μsec at $x = -17.1$ cm; 815 μsec

Table 1 The initial and condensation onset conditions for a selected number of experimental runs with P_{v4} the initial vapor pressure in driver

	Initial conditions[a]					Onset conditions[a]					
						$x = -17.1$ cm			$x = -35.1$ cm		
Experimental run no.	P_{v4} mm Hg	P_4 mm Hg	T_4 K	ϕ_4 %	ω_4	P_{vc} mm	T_c K	S	P_{vc}	T_c	S
29	15.4	650	296.4	75.4	0.0154	8.81	252.24	12.34	9.67	259.35	6.93
36	15.1	400	297.8	68.1	0.0246	8.95	256.10	8.69	9.36	259.53	6.59
41	15.8	680	295.0	84.1	0.0151	9.04	251.20	14.00	10.01	258.74	7.59
42	17.1	680	295.2	89.9	0.0163	9.98	252.87	13.15	10.89	259.27	7.86
44	18.6	680	295.3	97.2	0.0178	10.91	253.33	13.75	12.61	264.06	5.91
47	18.4	600	295.7	93.9	0.0199	10.49	251.54	15.72	11.62	259.12	8.50
48	20.7	600	297.7	93.6	0.0225	11.90	253.92	14.17	15.04	271.65	3.67
50	10.6	680	293.5	61.7	0.0101	5.83	247.2	13.41	6.15	251.01	9.70

[a] P_4, T_4, φ_4, ω_4 are the initial pressure, temperature, relative humidity, and mass fraction, respectively. P_c, T_c, and S are the pressure, temperature, and ratio of the pressure at saturation to that of actual condensation.

Table 2 Theoretical and experimental sound velocities for various experimental runs

Experimental run number	Sound velocity (m/sec)		
	$a_{calculated}$	$a_{measured}$	$a_{saturation}$
29	352.58	352.94	334.25
36	354.13	354.33	329.27
41	351.73	351.56	340.65
42	351.94	352.25	345.36
44	352.11	352.25	349.99
47	352.52	352.10	348.29
48	353.93	353.63	349.68
50	350.50	351.56	344.89

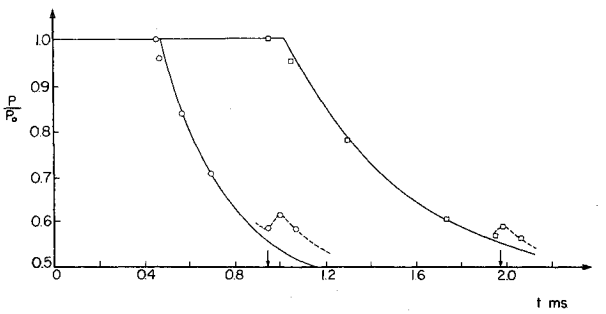

Fig. 6 Theoretical and experimental pressure-time profiles. $P_4 = 680$ Torr, $T_4 = 293.5$ K, $\phi_4 = 61.7\%$. – theoretical isentropes; o experimental points at location x_1; □ experimental points at location x_2;--pressure bump due to condensation and departure from isentrope.

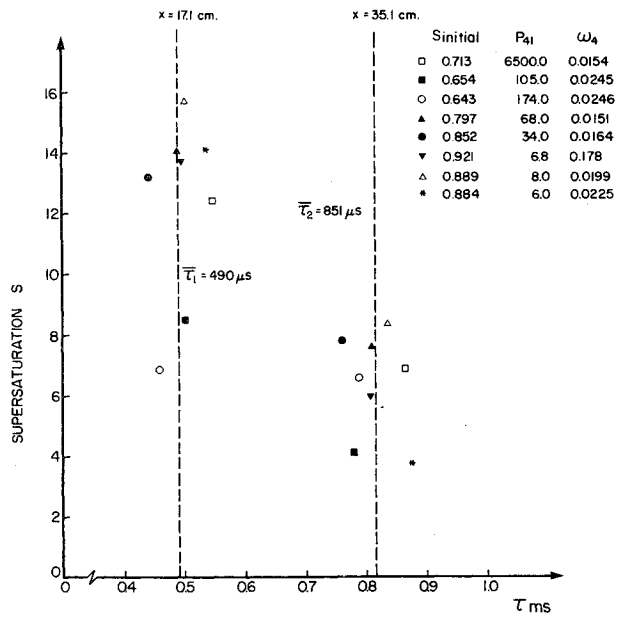

Fig. 7 Experimental results showing supersaturation S vs condensation delay time τ, and its mean value at $x_1 = -17.1$ cm and $x_2 = -35.1$ cm.

at $x = -35.1$ cm, as shown by the dashed lines; that is, near the diaphragm, τ is 40% smaller. As can be seen from Fig. 3, the measured laboratory time delays τ are longer than the actual dwell time along a particle path from the wave head to the onset of condensation.

In Fig. 8 the solid circles represent the nondimensional adiabatic supercooling defined as $\Delta = (T_s - T_c)/T_s$, where T_s is the saturation temperature and T_c the temperature at which condensation first occurs along a particle path, *computed at observed onset points* for a number of experimental runs as a function of the rate of cooling dT/dt in degrees K per second *at these points* in the rarefaction wave. The temperatures were determined from digitized (accuracy of 0.5%) pressure profiles. The error in Δ due to cancellations in the temperature ratio is much less than 2% and has a negligible effect on the location of the condensation front. At an infinite distance from the diaphragm[15] $dT/dt = 0$, and the flow is in equilibrium, so that $\Delta = 0$ there. A curve fit to the experimental data of the form $\Delta = C(-dT/dt)^n$ satisfying the conditions at $\Delta = 0$ and going through the experimental points yielded the realtion

$$\Delta = 1.73 \times 10^{-3} \left[-\frac{dT}{dt} \right]^{0.39} \tag{8}$$

Equation (8) is not applicable for high values of dT/dt and Δ at the onset of condensation close to the origin where the flow is in a near-frozen state. In the limiting case of a complete rarefaction wave $T_c = 0$, and $\Delta = 1$ for $dT/dt \to \infty$. Hence an exact curve of the type drawn in Fig. 8 would asymptotically approach the horizontal line $\Delta = 1$ for large values dT/dt. A similar type of relation was used by Smith[19] in steady expansion flows. However, his cooling rates were an order greater (0.3 to 3K/μsec) compared to ours (0.04 to 1K/μsec). Since his values of T_s are not known a direct comparison was not possible.

It has been shown in Ref. 11 that this empirical relation does not agree quantitatively with either homogeneous or heterogeneous models of nucleation. It is not clear whether this is due to the inadequacies of the models, uncertainties in the values of some of the droplet parameters or the nonideal experimental conditions. Nevertheless, Eq. (8) is useful for a qualitative parametric study of the location of the condensation front in the rarefaction fan.

Analysis of the Condensation Front Location

By assuming isentropic flow until the onset of condensation, Eq. (8) may be used to derive a relation for the path of the condensation front in the (x,t)-plane. The cooling rate that a fluid particle of the gas mixture would experience on passing through the nonstationary rarefaction wave can be given by

$$1 - \alpha(N+1) = \alpha(\delta - N), \quad N - \beta(N+1) = -\alpha(\delta - N)$$

as

$$\frac{1}{T_4}\frac{dT}{dt} = -\frac{2\alpha^3}{t}(N-\delta)^2 \tag{9}$$

where $\alpha = (\gamma_4 - 1)/(\gamma_4 + 1)$, $\beta = 2/(\gamma_4 + 1)$ and $N = x/a_4 t$. In addition,[15]

$$\frac{T}{T_4} = \left(\frac{a}{a_4}\right)^2 = \alpha^2(\delta - N)^2, \quad \delta = \frac{2}{\gamma_4 - 1}$$

Hence

$$\Delta = 1 - \frac{T_c}{T_s} = 1 - \left(\frac{\delta - N}{\delta - N_s}\right)^2 \tag{10}$$

where $N_s = x_s/a_4 t_s$ is the nondimensional slope of the saturation characteristic. The equation for the path of the condensation front can be obtained by substituting Eqs. (9) and (10) into Eq. (8)

$$1 - \left(\frac{\delta - N}{\delta - N_s}\right)^2 = 1.73 \times 10^{-3} \left\{ \frac{2T_4\alpha^3}{t}(N-\delta)^2 \right\}^{0.39} \tag{11}$$

It is seen that when $t \to \infty$, i.e. when $dT/dt \to 0$ (equilibrium condensation) the condensation front approaches asymptotically the saturation characteristic, $N \to N_s$ (Fig. 9b). It should be kept in mind that Eq. (11) is valid only for values of Δ and dT/dt shown in Fig. 8, and does not describe adequately the condensation front near the origin when $t \to 0$,

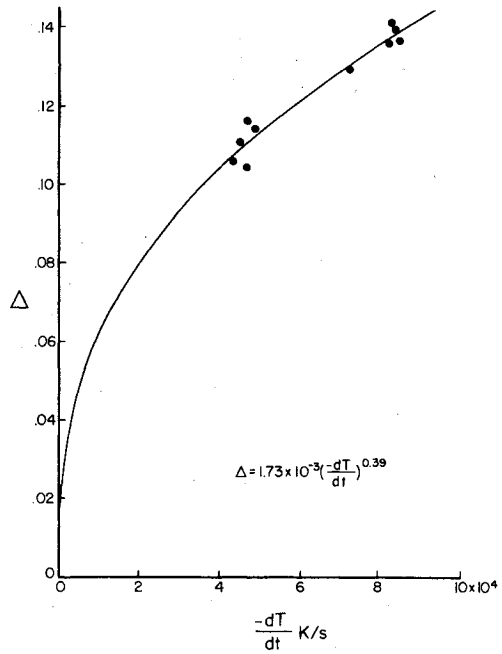

Fig. 8 Plot of nondimensional supercooling Δ and rate of cooling dT/dt.

$-dT/dt \to \infty$ and $\Delta \to 1$, and the flow is in the near-frozen condition.

It can be shown that for a gas mixture of constant γ the condensation front, in the near-frozen-flow region described by a relationship of functional form $\Delta = f(dT/dt)$ is *asymptotically* tangent to the tail of a complete rarefaction wave at the origin 0 (Fig. 9b). The point 0 itself is a singular point and is never attained.

The velocity of the front can be obtained from Eq. (11) as

$$\frac{dx}{dt} = U = \frac{x}{t} - \frac{0.39 a_4 \Delta (N-\delta)}{2[(1-\Delta)+0.39\Delta]} \tag{12}$$

If u and a are the fluid particle velocity and the speed of sound just before the condensation front, then the Mach number relative to the front is given by

$$M = (u-U)/a$$

Equation (12) shows that the location of the condensation front depends on ω_4 (through γ_4 and a_4), T_4 and $N_s = x_s/a_4 t_s$. It can be shown that for fixed values of T_4 and ω_4, the quantity N_s depends only on ϕ_4, the relative humidity of the water vapor in the driver, in the following way:

$$\phi_4 = 10^{A(1-1/\bar{T}_s)}$$

where

$$\bar{T}_s = T_s/T_4 = [1-\alpha(N_s+1)]^2$$

and $A = 2263/T_4$ (Ref. 13). Hence the location of the condensation front depends only on T_4, ω_4 and ϕ_4, i.e., the initial conditions of the mixture in the driver.

As an example, Fig. 9 shows the paths of the condensation fronts in the (x,t)-plane, where T_4 and ω_4 are kept constant and φ_4 is varied. The corresponding rarefaction wave head (only one occurs since a_4 is independent of φ_4) and the saturation characteristics are shown for a ready estimate of the magnitude of the departure from equilibrium conditions. It is seen that the effect of varying φ_4 on the location of the condensation front in the rarefaction fan is quite significant. Decreasing the initial relative humidity φ_4 from 97% to 40% increases the condensation delay time by 39% at $x = -20$ cm. The delay times are measured in laboratory coordintes shown in Fig. 3. Computations show that at this same location, an

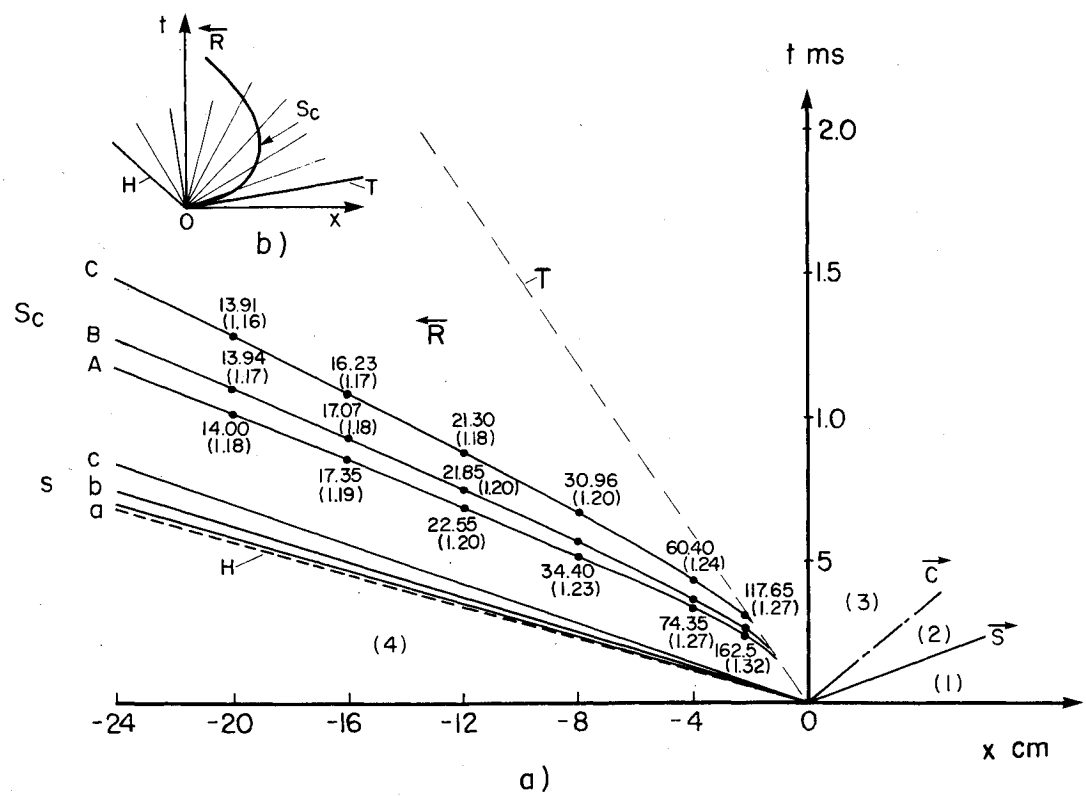

Fig. 9 Effects of relative humdiity φ_4 on condensation shock-wave path S_c: a) Supersaturation S (upper numbers) and Mach number M (brackets) are also shown at various path locations; $\omega_4 = 0.0177$, $T_4 = 295.3$K; values of φ_4 on paths A, B and C are 97.3%, 70% and 40%, respectively; corresponding saturation characteristics s are shown as a, b, and c; the isentropic wave tail is shown for a frozen Mach number $M_f = 0.784$. b) Condensation path for a complete wave.

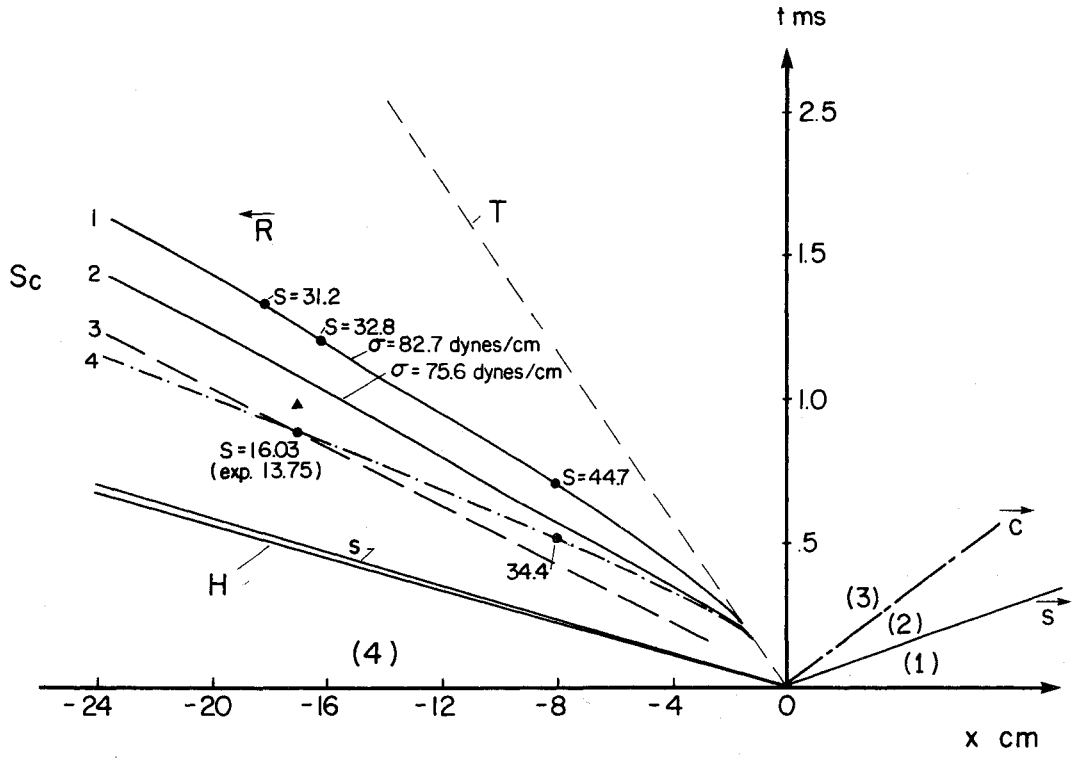

Fig. 10 A comparison of experimental and theoretical condensation shock wave paths: T = frozen isentropic wave tail $M_f = 0.784$, H = wave head, s = saturation characteristic, S_c = condensation shock wave paths; 1, 2 = method of characteristics (Ref. 11) for specific values of supersaturation S, and surface tension σ, 3 = averaged path from three schlieren records shown in Fig. 4, ▲ onset of condensation from present pressure record, 4 = path predicted by empirical relation, Eq. (8).

increase of ω_4 by about two orders of magnitude increases the condensation delay time by only ~7%. If T_4 is increased from 295K to 400K a 13% increase is predicted for the condensation delay time. Also shown in Fig. 9 are the supersaturation S and the condensation wave Mach number (in brackets) at various locations in the driver.

For the initial parameters $\omega_4 = 0.017$, $\varphi_4 = 0.97$, $T_4 = 295.3$K, and $P_{41} = 6.8$, Fig. 10 shows the paths of the homogeneous condensation wave calculated analytically[12] for two values of the surface tension, and the empirically determined path, using Eq. (11). Also shown are a typical experimental condensation onset point from the pressure records and the averaged schlieren path of the condensation front shown in Fig. 4 obtained for initial conditions very close to the ones considered here. Although the agreement between the schlieren path and the empirical prediction is satisfactory, the more rigorous analytical[11,12] results indicate higher values of condensation delay times. Data presented in Ref. 13 indicate that if a sufficient number of foreign nuclei are present (the so-called Aitken nuclei[11]) in the mixture, the condensation process takes place closer to the saturation characteristic rather than the condensation fronts predicted by the homogeneous condensation process. This trend is in line with the present experimental observations. Additional experimental details can be found in Ref. 20.

Conclusions

The detailed analytical predictions of homogeneous and heterogeneous condensation processes in rarefaction-wave flows are only in qualitative agreement with the present experiments. The experimental results can be brought into agreement with the theoretical predictions by an appropriate but arbitrary choice of the surface tension[12] and the contact angle of embryos.[11] However, this is not a satisfactory procedure. Consequently, experiments are still needed to settle the applicability of the heterogeneous or the homogeneous condensation model and the magnitudes of the physical parameters of the surface tension and the contact angles involved. Both condensation processes probably take place simultaneously when Aitken nuclei are not removed by electronic or other means.

In the meantime the analytical tools have been developed that have taken into account what is known today from kinetic theory, continuum, and empirical viewpoints. These should be valuable guides for future decisive experiments in this area as well as for a critical comparison of condensation in steady and nonstationary flows.

Acknowledgments

The financial support received from the National Research Council of Canada, the Aomic Energy of Canada Ltd. (Chalk River) and the U.S. Air Force Office of Scientific Research (AF-FOSR 72-2274) is acknowledged with thanks.

References

[1]Hill, P. G., "Condensation of Water Vapour During Supersonic Expansion in Nozzles," *Journal of Fluid Mechanics*, Vol. 25, Part 1, 1966, pp. 593-620.

[2]Wegener, P. P. and Mach, L. M., "Condensation in Supersonic and Hypersonic Wind Tunnels," *Advances in Applied Mechanics*, Vol. 5, 1958, pp. 307-447.

[3]Daum, F. L. and Gyarmathy, G., "Condensation of Air and Nitrogen in Hypersonic Wind Tunnels," *AIAA Journal*, Vol. 6, March 1968, pp. 458-465.

[4]Courtney, W. G., "Condensation in a Rarefaction Wave," Technical Supplement No. 2, Office of Naval Research ONR NR 092-517/4-29-65, Thiokol Chemical Corporation, Denville, N.J., Dec. 1965.

[5]Wegener, P. P. and Lundquist, G., "Condensation of Water Vapor in the Shock Tube below 150°K," *Journal of Applied Physics*, Vol. 22, Feb. 1951, p. 233.

[6]Glass, I. I. and Patterson, G. N., "A Theoretical and Experimental Study of Shock-Tube Flows," *Journal of the Aeronautical Sciences*, Vol. 22, Feb. 1955, pp. 73-100; see also Glass, I. I., Martin, W. A. and Patterson, G. N., "A Theoretical and Experimental Study

of the Shock Tube," University of Toronto, Institute for Aerospace Studies, Report No. 2, Nov. 1953.

[7]Homer, J. B., "Studies on the Nucleation and Growth of Metallic Particles from Supersaturated Vapors," *Shock Tube Research, Proceedings of the Eighth International Shock Tube Symposium, London*, edited by J. L. Stollery, A. G. Gaydon and P. R. Owen, Chapman and Hall, London, 1971.

[8]Kung, R. T. V. and Bauer, S. H., "Nucleation Rates in Fe Vapor: Condensation to Liquid in Shock Tube Flow," *Shock Tube Research*, ibid.

[9]Kawada, H. and Mori, Y., "A Shock Tube Study on Condensation Kinetics," *Bulletin of the Japan Society of Mechanical Engineers*, Vol. 16, July 1973, pp. 1053-1065.

[10]Barschdorff, D., "Carrier Gas Effects on Homogeneous Nucleation of Water Vapor in a Shock Tube," *The Physics of Fluids*, Vol. 18, May 1975, pp. 529-535.

[11]Kotake, S. and Glass, I. I., "Condensation of Water Vapor in Rarefaction Waves—II. Heterogeneous Nucleation," *AIAA Journal*, Vol. 15, Feb. 1977, pp. 215-221;(see also "Condensation of Water Vapor on Hetrogeneous Nuclei in a Shock Tube," University of Toronto, Institute for Aerospace Studies, Rept. No. 207, April 1976).

[12]Sislian, J. P. and Glass, I. I., "Condensation of Water Vapor in Rarefaction Waves—I. Homogeneous Nucleation," *AIAA Journal*, Vol. 14, Dec. 1976, pp. 1731-1737.

[13]Wegener, P. P., "Gasdynamics of Expansion Flows with Condensation and Homogeneous Nucleation of Water Vapour," *Nonequilibrium Flow*, Ch. 4, Part 1, edited by P. P. Wegener, Marcel Dekker, Inc., New York, 1970.

[14]Kalra, S. P., "Atomic Collisional Rate and Ionization Relaxation Study in a Helium Shock Wave," University of Toronto, Institute for Aerospace Studies, Report No. 181, March 1972.

[15]Glass, I. I. and Hall, J. G., "Handbook of Supersonic Aerodynamics," Section 18, Shock Tubes, NAVORD Report 1488, Vol. 6, U.S. Government Printing Office, Washington 25, D.C., Dec. 1959.

[16]Glass, I. I., "On the Speed of Sound in Gases," *Journal of the Aeronautical Sciences*, Vol. 14, April 1952, p. 286.

[17]Hall, J. G., Srinivasan, G. and Rathi, J. S., "Unsteady Expansion Waveforms Generated by Diaphragm Rupture," *AIAA Journal*, Vol. 12, May 1974, pp. 724-726.

[18]Barrand, J. P. and Rieutord, E., "Study of the Condensation of Water Vapour During Unsteady Discharge in a Long Tube," (in French), *International Journal of Heat Mass Transfer*, Vol. 16, Jan. 1973, pp. 101-108.

[19]Smith, L. T., "Experimental Investigation of the Expansion of Moist Air Around a Sharp Corner," *AIAA Journal*, Vol. 9, Oct. 1971, pp. 2035-2037.

[20]Kalra, S. P., "Experiments on Nonequilibrium, Nonstationary Expansion of Water Vapor/Carrier Gas Mixture in a Shock Tube," University of Toronto, Institute for Aerospace Studies, Rept. No. 195, April 1975.